Logical Magic State Preparation with Fidelity beyond the Distillation Threshold on a Superconducting Quantum Processor

Yangsen Ye,[1,2,*] Tan He,[1,2,*] He-Liang Huang,[1,2,3,*] Zuolin Wei,[1,2] Yiming Zhang,[1,2] Youwei Zhao,[1,2] Dachao Wu,[1,2]
Qingling Zhu,[2,4] Huijie Guan,[1,2] Sirui Cao,[1,2] Fusheng Chen,[2,4] Tung-Hsun Chung,[2,4] Hui Deng,[1,2,4] Daojin Fan,[1,2]
Ming Gong,[1,2,4] Cheng Guo,[1,2] Shaojun Guo,[1,2] Lianchen Han,[1,2] Na Li,[1,2] Shaowei Li,[2,4] Yuan Li,[1,2] Futian Liang,[1,2,4]
Jin Lin,[2,4] Haoran Qian,[1,2] Hao Rong,[1,2] Hong Su,[1,2] Shiyu Wang,[1,2] Yulin Wu,[1,2] Yu Xu,[2,4] Chong Ying,[1,2]
Jiale Yu,[1,2] Chen Zha,[2,4] Kaili Zhang,[2] Yong-Heng Huo,[1,2,4] Chao-Yang Lu,[1,2,4] Cheng-Zhi Peng,[1,2,4]
Xiaobo Zhu⊙,[1,2,4] and Jian-Wei Pan[1,2,4]

[1]*Hefei National Research Center for Physical Sciences at the Microscale and School of Physical Sciences,*
University of Science and Technology of China, Hefei 230026, China
[2]*Shanghai Research Center for Quantum Science and CAS Center for Excellence in Quantum Information and Quantum Physics,*
University of Science and Technology of China, Shanghai 201315, China
[3]*Henan Key Laboratory of Quantum Information and Cryptography, Zhengzhou, Henan 450000, China*
[4]*Hefei National Laboratory, University of Science and Technology of China, Hefei 230088, China*

Fault-tolerant quantum computing based on surface code has emerged as an attractive candidate for practical large-scale quantum computers to achieve robust noise resistance. To achieve universality, magic states preparation is a commonly approach for introducing non-Clifford gates. Here, we present a hardware-efficient and scalable protocol for arbitrary logical state preparation for the rotated surface code, and further experimentally implement it on the *Zuchongzhi* 2.1 superconducting quantum processor. An average of 0.8983 ± 0.0002 logical fidelity at different logical states with distance three is achieved, taking into account both state preparation and measurement errors. In particular, the logical magic states $|A^{\pi/4}\rangle_L$, $|H\rangle_L$, and $|T\rangle_L$ are prepared nondestructively with logical fidelities of 0.8771 ± 0.0009, 0.9090 ± 0.0009, and 0.8890 ± 0.0010, respectively, which are higher than the state distillation protocol threshold, 0.859 (for H-type magic state) and 0.827 (for T-type magic state). Our work provides a viable and efficient avenue for generating high-fidelity raw logical magic states, which is essential for realizing non-Clifford logical gates in the surface code.

Introduction.—Practical quantum computers are extremely difficult to engineer and build, as they are easily crippled by the inevitable noise in realistic quantum hardware [1,2]. Fault-tolerant quantum computing building on quantum error correction (QEC) offers a promising path to quantum computation at scale, by encoding the quantum information into logical qubits. In the past decades, much progress has been made to construct QEC schemes and realize QEC in the specific context of trapped ions [3–6], superconducting circuits [7–16], photons [17–20], and nitrogen-vacancy centers [21–23]. The surface code [24–26], a planar realization of Kitaev's toric code, is experimentally attractive as it requires only a two-dimensional lattice of qubits with nearest-neighbour coupling, and has a high error threshold of about 1%. The quality properties and great potential of surface code have driven efforts to scale up experiments from distance two [7–9] to distance three [10,11] and even distance five [12], until reaching a practical level.

Working with logical qubits to achieve a specific computational task introduces additional overhead for logical quantum gate operations. The surface code provides a relatively low-overhead implementation of the logical Clifford gate. However, a quantum circuit consisting of only Clifford gates is not computationally universal, nor does it confer any quantum computational advantage, since it can be efficiently simulated by classical computing [27,28]. In order to achieve computational universality, there must be at least one non-Clifford gate, such as a T gate. These non-Clifford gates can be implemented through magic state injection [29–35], but, unfortunately, it takes a large overhead and a huge number of magic states [31,32,34,36,37]. Thus, fast and high-fidelity logical magic state preparation [38–40] is crucial in the implementation of universal logical quantum gates.

This work aims to explore how to prepare an arbitrary logical state, especially magic states, quickly and with high fidelity. Specifically, an arbitrary logical state preparation protocol is proposed for the rotated surface code, inspired by some relevant works [38,39]. The protocol does not require extra ancilla qubits and is almost identical to the standard surface code protocol, except that the quantum
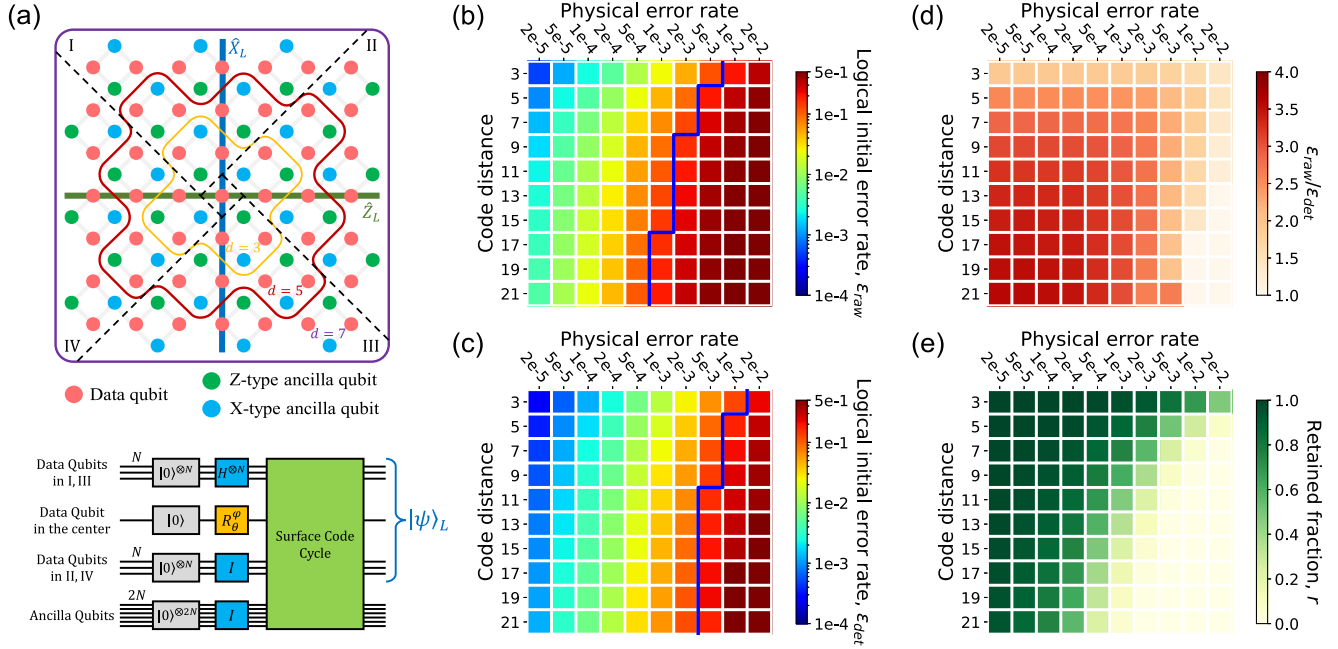
FIG. 1. Arbitrary logical state preparation protocol and simulation results. (a) Arbitrary logical state preparation protocol. Top panel: The surface code is divided into 5 regions, the central data qubit, regions I, II, III, and IV. The logical operators $\hat{Z}_L$ and $\hat{X}_L$ intersect at the central data qubits. Bottom panel: The circuit of the protocol. All qubits are reset to the $|0\rangle$ state at the beginning of the circuit. Then the data qubits in the regions I and III are prepared in the $|+\rangle$ state by Hadamard gate, and the central data qubit is prepared in the target state $|\psi\rangle$ by rotation gates. One round of surface code cycle is applied afterwards, projecting the data qubits state into the logical state space. (b)–(e) Simulation results for the $|+i\rangle_L$ state preparation. (b)–(c) Logical initial error rate as a function of average physical error rate and surface code distance with no postprocessing (b) and with postselection of only syndrome measurements (c). The blue lines in the figure indicate the most demanding error threshold, 0.141 (equals to 1-0.859, where 0.859 is the fidelity threshold of the 15-to-1 state distillation protocol for the H-type magic state), for state distillation protocol. (d)–(e) The ratio of $\varepsilon_{\rm raw}$ to $\varepsilon_{\rm det}$ and the retained fraction of postselection as a function of average physical error rate and surface code distance.

state needs to be prepared to a specific product state according to the target logical state during the initialization stage. Theoretical analysis shows good scaling behavior of the protocol for high-fidelity large-scale logical quantum state preparation (see analysis in the Supplemental Material [41]). Furthermore, we experimentally realize the protocol on the *Zuchongzhi* 2.1 superconducting quantum system [45,46] to demonstrate its practical performance on real quantum devices. An average logical fidelity of 0.8983 ± 0.0002 is achieved with postselection using syndrome measurements for different prepared logical states, even in the presence of significant readout errors during measurement. Among them, two H-type logical magic states $|A^{\pi/4}\rangle_L$, $|H\rangle_L$ and one T-type logical magic state $|T\rangle_L$ are obtained with logical fidelities of 0.8771 ± 0.0009, 0.9090 ± 0.0009, and 0.8890 ± 0.0010, respectively. These are significantly higher than the 15-to-1 magic state distillation protocol threshold 0.859 (for H-type magic state) and the 5-to-1 magic state distillation protocol threshold 0.827 (for T-type magic state) [29]. Here the threshold indicates the minimum allowable fidelity of the input raw magic states that can be successfully distilled to a higher-fidelity magic state through the protocol. The achieved results suggest that our work represents a key

step towards universal and scalable fault-tolerant quantum computing, and has the potential to play a crucial role in some NISQ protocols or algorithms [47–55], such as error mitigation [56,57].

Arbitrary logical state preparation protocol.—The arbitrary logical state preparation protocol is shown in Fig. 1(a). The basic idea is to initialize the data qubits to a specific quantum state first, and then apply one round surface code cycle to project the data qubits into the logical state space. Assume the target logical state is $|\psi\rangle_L = \alpha|0\rangle_L + \beta|1\rangle_L$, the detailed steps of our protocol can be described in the following: (1) Reset all qubits to the $|0\rangle$ state, including data qubits and ancilla qubits. (2) Divide the rotated surface code into 5 regions, the central data qubit, regions I, II, III, and IV, as shown in the top panel of Fig. 1(a). Prepare the data qubits in regions I and III in the $|+\rangle$ state and the data qubit in the center (intersection of logical operators $\hat{Z}_L$ and $\hat{X}_L$) in the target state $|\psi\rangle = \alpha|0\rangle + \beta|1\rangle$, while the data qubits of the remaining regions II and IV stay in the $|0\rangle$ state. The data qubit state after step 2 is

$$|\Psi_0\rangle = |\psi\rangle \bigotimes_{D_i \in {\rm I}\cup{\rm III}} |+\rangle \bigotimes_{D_j \in {\rm II}\cup{\rm IV}} |0\rangle, \qquad (1)$$

where $D_i \in \mathrm{I} \cup \mathrm{III}$ ($D_j \in \mathrm{II} \cup \mathrm{IV}$) is denoted as the data qubit of region I and III (II and IV). (3) Apply one round of surface code cycle. After measuring all the ancilla qubits, the data qubits are then prepared in the desired logical state $|\psi\rangle_L$.

The protocol is applicable to the surface code with arbitrary distance d, and its quantum circuit is shown in the bottom panel of Fig. 1(a). The X stabilizers in regions I and III and the Z stabilizers in regions II and IV would have the deterministic measurement values 0 if no error occurred. With postselection procedures using these stabilizers, the logical initial error rate can be effectively reduced.

We further investigate the performance of the protocol through numerical simulation [see Figs. 1(b)–1(e)]. We consider circuit-level noise and characterize it with the depolarizing noise model. In addition, we use the average physical error rate; i.e., the error rate of all operations, including single-qubit gate, two-qubit gate, readout, and thermal excitation, is the same. The target logical state we choose in simulation is $|+i\rangle_L$, and by doing so, the error detection capabilities of X and Z stabilizers can be tested simultaneously.

We simulate the logical initial error rate with different surface code distances and physical error rates. The simulated circuits contain only one round of surface code cycle [as shown in Fig. 1(a)], followed by a logical Y measurement (see details in the Supplemental Material [41]). The readout error for data qubits was set to zero to obtain the logical state preparation fidelity without readout errors. The results without any postprocessing and with syndrome measurement postselection are shown in Figs. 1(b) and 1(c), respectively. The blue line indicates the threshold for state distillation protocol of the magic state, the threshold here is chosen to be the most demanding 15-to-1 H-type protocol threshold of 0.141. As we can see, the logical initialization error rate increases with the increasing of the surface code distance and the average physical error rate. It is clear that there is a significant decrease in the logical error rate by the postselection, and the blue line is thus moved towards the right, which means that more relaxed conditions are able to perform the state distillation procedure. Figure 1(d) shows the ratio of logical initial error rate before and after postselection, which represents the suppression ability of the postselection for errors in the logical state preparation process. It can be seen that the suppression rate ranges from 1 to 4 times for different conditions, and the suppression ability becomes stronger as the code distance grows and the average physical error rate decreases.

The retained fraction of postselection is shown in Fig. 1(e). This is an important indicator for the efficiency of state distillation. The retained fraction increases with decreasing code spacing and average physical error rate. When the average error rate is 0.0002, the retained fraction is acceptable in state distillation even for a code distance-21 (about 56%).
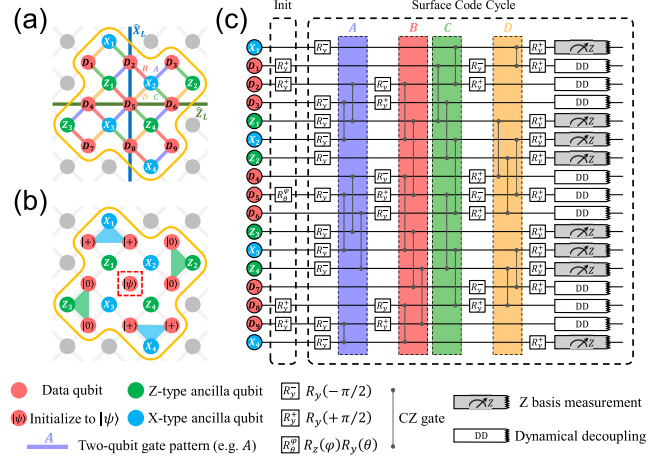

FIG. 2. Layout and circuit implementation. (a) Structure of distance-three surface code, with 9 data qubits (red dots), 4 Z-type ancilla qubits (green dots), and 4 X-type ancilla qubits (blue dots). Connecting lines are colored according to their involvement in two-qubit gate layers as shown in (c). (b) Preparing 9 data qubits to a specific state, with 4 qubits stay in the $|0\rangle$ state, 4 qubits initialize to the $|+\rangle$ state and only one qubit transform to the target $|\psi\rangle$ state. (c) Circuit for preparing arbitrary logical state. First initialize 9 data qubits to specific states as (b) illustrated, then apply one round surface code cycle. Squares with different tags represent different single-qubit gates. All gates in one color block are applied simultaneously.

Experimental implementation on a superconducting quantum processor.—To demonstrate the performance of the protocol on a real quantum device, we create a distance-three surface code using 17 out of the 66 qubits on the *Zuchongzhi* 2.1 superconducting quantum system. We present the system performance in the Supplemental Material [41]. This 17-qubit distance-three surface code [see Fig. 2(a)] consists of 9 data qubits, 4 X-type ancilla qubits, and 4 Z-type ancilla qubits. To prepare the logical state $|\psi\rangle_L = \cos(\theta/2)|0\rangle_L + e^{i\varphi}\sin(\theta/2)|1\rangle_L$, the data qubits are initialized in the way shown in Fig. 2(b) to the product state

$$|\Psi\rangle = |+\rangle|+\rangle|0\rangle|0\rangle|\psi\rangle|0\rangle|0\rangle|+\rangle|+\rangle, \qquad (2)$$

where $|\psi\rangle = \cos(\theta/2)|0\rangle + e^{i\varphi}\sin(\theta/2)|1\rangle$ can be experimentally realized using the virtual Z gate and standard $\pi/2$ gate, as

$$|\psi\rangle = Z_\varphi \cdot X_{\pi/2} \cdot Z_{\pi-\theta} \cdot X_{\pi/2}|0\rangle. \qquad (3)$$

The corresponding quantum circuit is shown in Fig. 2(c). After implementing one round of surface code cycle, the logical state $|\psi\rangle_L$ is prepared. Furthermore, as shown in Fig. 2(b), in the logical state preparation process, 4 stabilizers X_1, Z_2, Z_3, X_4 are deterministic.

We first prepare different logical states of uniformly scattered points on the Bloch sphere by varying the
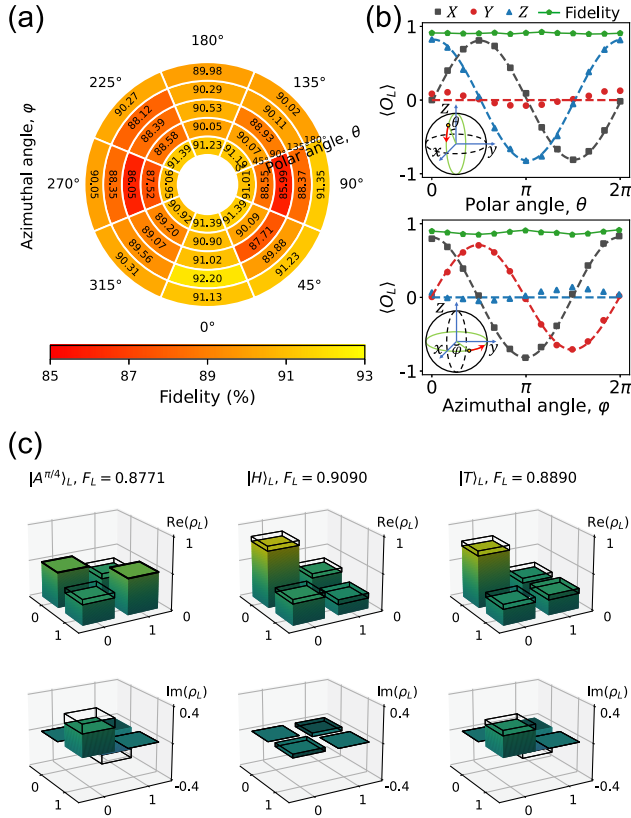
FIG. 3. Experimental results for preparing different logical states. (a) Logical state fidelities with postselection in Bloch sphere. The fidelities of the preparation of different logical states are represented as a circle, which is divided into multiple annular sectors, each representing a point on the Bloch sphere, with the radial direction representing the polar angle θ and the tangential direction representing the azimuthal angle φ. The obtained average logical fidelity is 0.8983. (b) Logical measurement results of X_L, Y_L, Z_L as a function of polar angle θ or azimuthal angle φ. The colored dashed curves are the result of fitting with trigonometric function. (c) The logical density matrices of the magic states. Real and imaginary parts are represented separately, and the transparent wire frames represent the difference from the ideal density matrix.

parameters of θ and φ. Figure 3(a) shows the logical state fidelities F_L of these prepared logical states after using postselection to drop the results that have detection events during the preparation (the raw logical fidelities are shown in Supplemental Material [41]), where

$$F_L = \left(\text{Tr} \sqrt{ \sqrt{\rho_{\text{exp}}} \cdot \rho_{\text{theory}} \cdot \sqrt{\rho_{\text{exp}}} } \right)^2, \quad (4)$$

and ρ_{exp} is the experimental density matrix reconstructed by maximum-likelihood estimation after logical X_L, Y_L, Z_L measurements. We note that the measurement results include both state preparation and measurement (SPAM) error. We do not employ readout error mitigation strategies

[58] to remove measurement errors because we believe it provides a more predictive assessment of the actual fidelity when generating and consuming magic states for a non-Clifford gate, as consuming the state involves measurement. These fidelities are represented as pie shaped [Fig. 3(a)], which is divided into multiple annular sectors, each representing a point on the Bloch sphere, with the radial direction representing the polar angle θ and the tangential direction representing the azimuthal angle φ. The obtained average logical fidelity is 0.8983 ± 0.0002. Furthermore, we fixed one parameter in θ and φ, measuring the logical operators $\hat{X}_L$, $\hat{Y}_L$, $\hat{Z}_L$ to obtain expectation results as a function of the other parameter. As shown in Fig. 3(b), the experimental points of $\langle X \rangle_L$, $\langle Y \rangle_L$, and $\langle Z \rangle_L$ are consistent with the sine or cosine variation.

Also, we show the quantum state tomography results of the three logical magic states, including two H-type magic states $|A^{\pi/4}\rangle_L = (1/\sqrt{2})(|0\rangle_L + e^{i\pi/4}|1\rangle_L)$ and $|H\rangle_L = \cos(\pi/8)|0\rangle_L + \sin(\pi/8)|1\rangle_L$, and one T-type magic state $|T\rangle_L = \cos(\beta/2)|0\rangle_L + e^{i\pi/4}\sin(\beta/2)|1\rangle_L$, where $\beta = \arccos(1/\sqrt{3})$. These two type magic states are the quantum resources for realizing non-Clifford gates $\Lambda(e^{-i\pi/4})$ and $\Lambda(e^{-i\pi/6})$, where

$$\Lambda(e^{-i\theta}) = \begin{pmatrix} 1 & 0 \\ 0 & e^{i\theta} \end{pmatrix}. \quad (5)$$

In Fig. 3(c), the real and imaginary parts of the density matrix are shown separately. The logical fidelities of these magic states are $|A^{\pi/4}\rangle_L$: 0.8771 ± 0.0009, $|H\rangle_L$: 0.9090 ± 0.0009, and $|T\rangle_L$: 0.8890 ± 0.0010, which exceed the threshold of the respective state distillation.

To observe the error correction performance of the surface code for different logical initial states, we repeatedly apply the surface code cycles after the logical state is prepared. Figure 4 shows how the fidelities of the logical states varies with the number of surface code cycles with and without error correction. The logical error rates are derived by fitting the curves with $\mathcal{F}_L(k) = \frac{1}{2}\left(1 + (1 - 2\epsilon_L)^{k-k_0}\right)$ [59]. Figures 4(a) and 4(c) show the results for the $|0\rangle_L$ and $|+\rangle_L$ using the arbitrary state preparation protocol. The logical error rates per round of the $|0\rangle_L$ and $|+\rangle_L$ are 28.53% and 32.24% without error correction. After the error correction procedure, the fidelities of the logical state at each cycle is improved and the logical error rates per round are reduced to 24.77% and 25.65%, respectively. As a comparison, the results using the standard protocol [26] for the $|0\rangle_L$ and $|+\rangle_L$ are shown in Figs. 4(b) and 4(d), and we can observe that the logical error rates per round of the two protocols are similar. The most obvious difference is that in the results obtained by standard protocol, the fidelities of the logical states at the first round is significantly improved with error correction. This is mainly because all the four stabilizers Z_1, Z_2, Z_3, Z_4
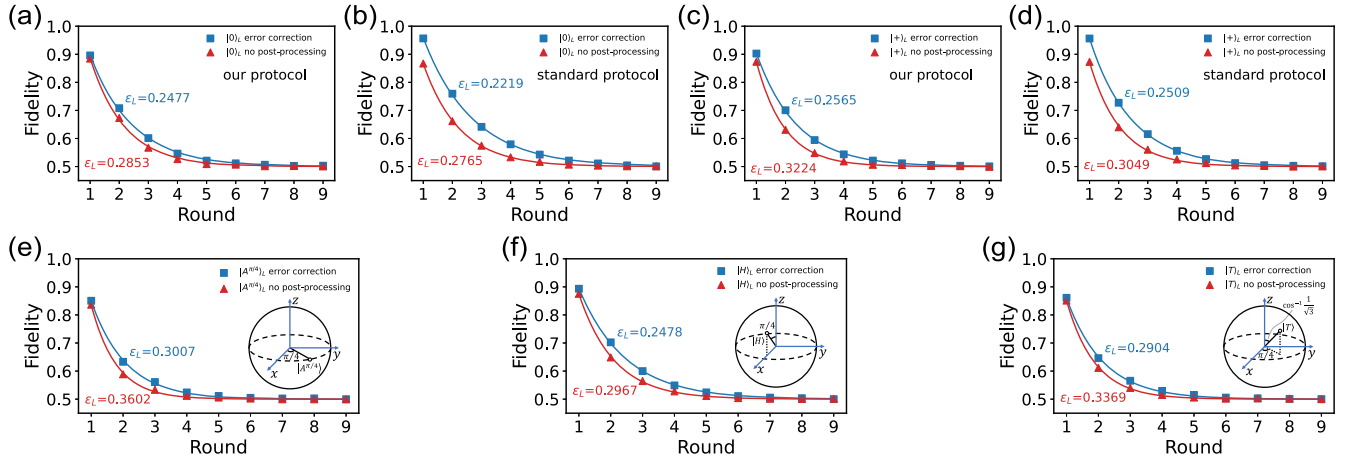
FIG. 4. Fidelities of different logical states with error correction. (a) and (b) The fidelities of the logical state $|0\rangle_L$ as a function of the number of surface code cycles with (blue line with square) and without (red line with triangular) error correction, by using arbitrary logical state preparation protocol (a) and standard protocol (b), respectively. (c)–(d) Same as (a)–(b) with the logical state $|+\rangle_L$. (e)–(g) Results for preparing the logical states $|A^{\pi/4}\rangle_L$, $|H\rangle_L$, and $|T\rangle_L$ using the arbitrary logical state preparation protocol, respectively.

(X_1, X_2, X_3, X_4) are work for the $|0\rangle_L$ ($|+\rangle_L$) in the first round, while only half of stabilizers, X_1 and X_4 (Z_2 and Z_3), work for the $|0\rangle_L$ ($|+\rangle_L$) in our arbitrary logical state preparation protocol [as shown in Fig. 2(b)]. These stabilizers are in the edge positions and not near neighbors, so it is difficult to correct error during logical state preparation. The most valuable aspect of the arbitrary logical state preparation protocol is that it can simply prepare arbitrary logical states, whereas the standard approach requires very complex operations. Figures 4(e)–4(g) show the results for the logical magic states $|A^{\pi/4}\rangle_L$, $|H\rangle_L$, and $|T\rangle_L$. The achieved results show that the logical error rates per round for these prepared complex logical states are comparable to that of the standard logical states.

Conclusion and outlook.—The crucial step for surface code based fault-tolerant computing, preparing distance-three logical magic state with fidelity beyond the distillation threshold, is achieved in this work. Our work provides a highly simple, experimentally friendly, and scalable way to prepare high-fidelity raw magic states, which is critical for decreasing the overhead for distillation, and thus paving the way for practical fault-tolerant quantum computing. The protocol developed is partially fault tolerant and naturally compatible with the error detection and repeated error correction, to enhance the logical state fidelity as well as to lift the logical coherence time. It might be improved to fully fault tolerant by introducing a flag qubit mechanism [60,61]. In addition, using some new approaches may further enhance the fidelity of magic state preparation and measurement [40,62]. All of these will be left for our future work.

*These authors contributed equally to this work.

[1] H.-L. Huang, D. Wu, D. Fan, and X. Zhu, Sci. China Inf. Sci. **63**, 180501 (2020).

[2] H.-L. Huang, X.-Y. Xu, C. Guo, G. Tian, S.-J. Wei, X. Sun, W.-S. Bao, and G.-L. Long, Sci. China Phys. Mech. Astron. **66**, 250302 (2023).

[3] P. Schindler, J. T. Barreiro, T. Monz, V. Nebendahl, D. Nigg, M. Chwalla, M. Hennrich, and R. Blatt, Science 332, 1059 (2011).

[4] L. Egan, D. M. Debroy, C. Noel, A. Risinger, D. Zhu, D. Biswas, M. Newman, M. Li, K. R. Brown, M. Cetina et al., Nature (London) 598, 281 (2021).

[5] C. Ryan-Anderson, J. G. Bohnet, K. Lee, D. Gresh, A. Hankin, J. P. Gaebler, D. Francois, A. Chernoguzov, D. Lucchetti, N. C. Brown, T. M. Gatterman, S. K. Halit, K. Gilmore, J. A. Gerber, B. Neyenhuis, D. Hayes, and R. P. Stutz, Phys. Rev. X 11, 041058 (2021).

[6] J. Hilder, D. Pijn, O. Onishchenko, A. Stahl, M. Orth, B. Lekitsch, A. Rodriguez-Blanco, M. Müller, F. Schmidt-Kaler, and U. G. Poschinger, Phys. Rev. X 12, 011032 (2022).

[7] C. K. Andersen, A. Remm, S. Lazar, S. Krinner, N. Lacroix, G. J. Norris, M. Gabureac, C. Eichler, and A. Wallraff, Nat. Phys. 16, 875 (2020).

[8] G. Q. AI, Nature (London) 595, 383 (2021).

[9] J. F. Marques, B. M. Varbanov, M. S. Moreira, H. Ali, N. Muthusubramanian, C. Zachariadis, F. Battistel, M. Beekman, N. Haider, W. Vlothuizen, A. Bruno, B. M. Terhal, and L. DiCarlo, Nat. Phys. 18, 80 (2021).

[10] Y. Zhao, Y. Ye, H.-L. Huang, Y. Zhang, D. Wu, H. Guan, Q. Zhu, Z. Wei, T. He, S. Cao, F. Chen et al., Phys. Rev. Lett. 129, 030501 (2022).

[11] S. Krinner, N. Lacroix, A. Remm, A. Di Paolo, E. Genois, C. Leroux, C. Hellings, S. Lazar, F. Swiadek, J. Herrmann et al., Nature (London) 605, 669 (2022).

[12] R. Acharya, I. Aleiner, R. Allen, T. I. Andersen, M. Ansmann, F. Arute, K. Arya, A. Asfaw, J. Atalaya, R. Babbush et al., Nature (London) 614, 676 (2023).

[13] M. D. Reed, L. DiCarlo, S. E. Nigg, L. Sun, L. Frunzio, S. M. Girvin, and R. J. Schoelkopf, Nature (London) 482, 382 (2012).

[14] N. Ofek, A. Petrenko, R. Heeres, P. Reinhold, Z. Leghtas, B. Vlastakis, Y. Liu, L. Frunzio, S. Girvin, L. Jiang et al., Nature (London) 536, 441 (2016).

[15] A. D. Córcoles, E. Magesan, S. J. Srinivasan, A. W. Cross, M. Steffen, J. M. Gambetta, and J. M. Chow, Nat. Commun. 6, 6979 (2015).

[16] H.-L. Huang, M. Narożniak, F. Liang, Y. Zhao, A. D. Castellano, M. Gong, Y. Wu, S. Wang, J. Lin, Y. Xu et al., Phys. Rev. Lett. 126, 090502 (2021).

[17] X.-C. Yao, T.-X. Wang, H.-Z. Chen, W.-B. Gao, A. G. Fowler, R. Raussendorf, Z.-B. Chen, N.-L. Liu, C.-Y. Lu, Y.-J. Deng et al., Nature (London) 482, 489 (2012).

[18] T. B. Pittman, B. C. Jacobs, and J. D. Franson, Phys. Rev. A 71, 052332 (2005).

[19] Y.-H. Luo, M.-C. Chen, M. Erhard, H.-S. Zhong, D. Wu, H.-Y. Tang, Q. Zhao, X.-L. Wang, K. Fujii, L. Li et al., Proc. Natl. Acad. Sci. U.S.A. 118, e2026250118 (2021).

[20] C. Liu, H.-L. Huang, C. Chen, B.-Y. Wang, X.-L. Wang, T. Yang, L. Li, N.-L. Liu, J. P. Dowling, T. Byrnes et al., Optica 6, 264 (2019).

[21] G. Waldherr, Y. Wang, S. Zaiser, M. Jamali, T. Schulte-Herbrüggen, H. Abe, T. Ohshima, J. Isoya, J. Du, P. Neumann et al., Nature (London) 506, 204 (2014).

[22] T. H. Taminiau, J. Cramer, T. van der Sar, V. V. Dobrovitski, and R. Hanson, Nat. Nanotechnol. 9, 171 (2014).

[23] J. Cramer, N. Kalb, M. A. Rol, B. Hensen, M. S. Blok, M. Markham, D. J. Twitchen, R. Hanson, and T. H. Taminiau, Nat. Commun. 7, 11526 (2016).

[24] A. Y. Kitaev, Ann. Phys. (Amsterdam) 303, 2 (2003).

[25] R. Raussendorf and J. Harrington, Phys. Rev. Lett. 98, 190504 (2007).

[26] A. G. Fowler, M. Mariantoni, J. M. Martinis, and A. N. Cleland, Phys. Rev. A 86, 032324 (2012).

[27] D. Gottesman, Group22: Proceedings of the XXII International Colloquium on Group Theoretical Methods in Physics (International Press, Cambridge, MA, 1999); arXiv:quant-ph/9807006.

[28] K. Bu and D. E. Koh, Phys. Rev. Lett. 123, 170502 (2019).

[29] S. Bravyi and A. Kitaev, Phys. Rev. A 71, 022316 (2005).

[30] B. W. Reichardt, Quantum Inf. Process. 4, 251 (2005).

[31] S. Bravyi and J. Haah, Phys. Rev. A 86, 052329 (2012).

[32] J. O'Gorman and E. T. Campbell, Phys. Rev. A 95, 032338 (2017).

[33] M. B. Hastings and J. Haah, Phys. Rev. Lett. 120, 050504 (2018).

[34] D. Litinski, Quantum 3, 205 (2019).

[35] J. Gavriel, D. Herr, A. Shaw, M. J. Bremner, A. Paler, and S. J. Devitt, Phys. Rev. Res. 5, 033019 (2023).

[36] A. G. Fowler and C. Gidney, arXiv:1808.06709.

[37] E. T. Campbell and M. Howard, Phys. Rev. A 95, 022316 (2017).

[38] Y. Li, New J. Phys. 17, 023037 (2015).

[39] J. Łodyga, P. Mazurek, A. Grudka, and M. Horodecki, Sci. Rep. 5, 8975 (2015).

[40] C. Gidney, arXiv:2302.12292.

[41] See Supplemental Material at http://link.aps.org/supplemental/10.1103/PhysRevLett.131.210603 for the theoretical analysis of the arbitrary logical state preparation protocol, for the scheme of logical Y measurement, for the Zuchongzhi 2.1 system performance and for the raw logical fidelities of different states preparation, which includes Refs. [42–44].

[42] S. S. Elder, C. S. Wang, P. Reinhold, C. T. Hann, K. S. Chou, B. J. Lester, S. Rosenblum, L. Frunzio, L. Jiang, and R. J. Schoelkopf, Phys. Rev. X 10, 011001 (2020).

[43] D. C. McKay, C. J. Wood, S. Sheldon, J. M. Chow, and J. M. Gambetta, Phys. Rev. A 96, 022330 (2017).

[44] C. Gidney, Quantum 5, 497 (2021).

[45] Y. Wu, W.-S. Bao, S. Cao, F. Chen, M.-C. Chen, X. Chen, T.-H. Chung, H. Deng, Y. Du, D. Fan et al., Phys. Rev. Lett. 127, 180501 (2021).

[46] Q. Zhu, S. Cao, F. Chen, M.-C. Chen, X. Chen, T.-H. Chung, H. Deng, Y. Du, D. Fan, M. Gong et al., Sci. Bull. 67, 240 (2022).

[47] A. Rolander, A. Kinos, and A. Walther, Phys. Rev. A 105, 062604 (2022).

[48] H.-L. Huang et al., Phys. Rev. Appl. 16, 024051 (2021).

[49] H.-L. Huang, X.-L. Wang, P. P. Rohde, Y.-H. Luo, Y.-W. Zhao, C. Liu, L. Li, N.-L. Liu, C.-Y. Lu, and J.-W. Pan, Optica 5, 193 (2018).

[50] J. Liu, K. H. Lim, K. L. Wood, W. Huang, C. Guo, and H.-L. Huang, Sci. China Phys. Mech. Astron. 64, 290311 (2021).

[51] H.-L. Huang, Q. Zhao, X. Ma, C. Liu, Z.-E. Su, X.-L. Wang, L. Li, N.-L. Liu, B. C. Sanders, C.-Y. Lu et al., Phys. Rev. Lett. 119, 050503 (2017).

[52] C. Ying, B. Cheng, Y. Zhao, H.-L. Huang, Y.-N. Zhang, M. Gong, Y. Wu, S. Wang, F. Liang, J. Lin, Y. Xu, H. Deng, H. Rong, C.-Z. Peng, M.-H. Yung, X. Zhu, and J.-W. Pan, Phys. Rev. Lett. **130**, 110601 (2023).

[53] C. Ding, X.-Y. Xu, S. Zhang, H.-L. Huang, and W.-S. Bao, Phys. Rev. A **106**, 042421 (2022).

[54] C. Ding, X.-Y. Xu, Y.-F. Niu, S. Zhang, H.-L. Huang, and W.-S. Bao, Quantum Sci. Technol. **8**, 035030 (2023).

[55] Y.-F. Niu, S. Zhang, C. Ding, W.-S. Bao, and H.-L. Huang, SciPost Phys. **14**, 132 (2023).

[56] R. Hicks, B. Kobrin, C. W. Bauer, and B. Nachman, Phys. Rev. A **105**, 012419 (2022).

[57] C. Ding, X.-Y. Xu, Y.-F. Niu, S. Zhang, W.-S. Bao, and H.-L. Huang, Sci. China Phys. Mech. Astron. **66**, 230311 (2023).

[58] A. W. Smith, K. E. Khosla, C. N. Self, and M. Kim, Sci. Adv. **7**, eabi8009 (2021).

[59] T. O'brien, B. Tarasinski, and L. DiCarlo, npj Quantum Inf. **3**, 39 (2017).

[60] C. Chamberland and K. Noh, npj Quantum Inf. **6**, 91 (2020).

[61] C. Chamberland and A. W. Cross, Quantum **3**, 143 (2019).

[62] C. Gidney, arXiv:2302.07395.